Available online at www.sciencedirect.com

jmr&t Journal of Materials Research and Technology

journal homepage: www.elsevier.com/locate/jmrt

Original Article

Impact of the laser scanning strategy on the quality of 17-4PH stainless steel parts manufactured by selective laser melting

Sara Giganto [a], *Susana Martínez-Pellitero* [a], *Joaquín Barreiro* [a], *Paola Leo* [b], *Mª Ángeles Castro-Sastre* [a,*]

[a] *Area of Manufacturing Engineering, Universidad de León, 24071 León, Spain*

[b] *Innovation Engineering Department, University of Salento, Via per Arnesano s.n., 73100 Lecce, Italy*

ARTICLE INFO

Article history:
Received 11 July 2022
Accepted 10 August 2022
Available online 18 August 2022

Keywords:
17-4PH stainless steel
Additive manufacturing (AM)
Laser scanning strategy
Mechanical properties
Porosity
Selective laser melting (SLM)

ABSTRACT

A significant correlation between scanning strategies and the quality of parts manufactured additively with Selective Laser Melting (SLM) technology is shown. Therefore, a in deep study of the influence of scanning strategy is of great value for the manufacturing process in order to promote SLM technology in applications with high service requirements. In particular, this research is carried out on 17-4PH stainless steel parts, which is an alloy widely used in sectors such as aerospace or automotive for its excellent mechanical properties. This research proposes to evaluate the properties of 17-4PH parts manufactured using three usual scanning strategies (normal, concentric and hexagonal) in order to optimize the SLM process depending on the final part application. According to the obtained results, the following general conclusions have been drawn. Hexagonal strategy can be considered the most appropriate in terms of porosity. Both hexagonal and normal strategy have good mechanical properties, as well as geometrical and dimensional quality. Regarding surface finish of top face (where the used scanning pattern is visible), normal strategy is the most appropriate. In general, concentric strategy presents different results from the others: larger and irregular pores, ductile tensile behaviour, low roughness on lateral faces, and high geometrical errors in samples with large scanning vectors. As a future work, it is proposed to manufacture SLM parts combining these strategies in order to improve their properties. In addition, it is proposed to evaluate the influence of different post-process operations on the quality of parts printed by SLM using different strategies.

* Corresponding author.
E-mail address: macass@unileon.es (M.Á. Castro-Sastre).

https://doi.org/10.1016/j.jmrt.2022.08.040

1. Introduction

Selective Laser Melting (SLM) is a promising Additive Manufacturing (AM) technique that enables manufacturing of complex functional metallic components. This process consists in melting particles selectively from a powder bed, layer by layer, using a high-energy laser beam. SLM technique produces parts from a wide range of novel high-performance materials, used for many applications in strategic areas, such as medical, automotive or aerospace [1]. However, industry adoption is currently hampered by several technical barriers, such as deformation and delamination of printed parts due to residual stresses induced by this manufacturing process. The scanning path of the laser beam affects the thermomechanical behaviour of the parts. Therefore, modifying the scanning pattern can be a method to reduce residual stresses and deformations since it influences the input distribution of heat intensity [2]. Likewise, variation of laser scanning strategy directly affects the part quality, in properties such as density, microstructural characteristics, surface quality or mechanical properties [3]. All this promotes the researchers' interest in studying this SLM process parameter.

Several researchers have focused on optimizing the normal scanning strategy (stripe scanning strategy) by studying the influence of its different parameters on the quality of the SLM parts. Gu and Chen [4] designed a hatch style in which the tracks in adjacent layers are staggered half the hatch distance and rotated 90° every two layers. This hatch style succeeded in manufacturing fully dense 316L stainless steel parts with high microstructural homogeneity. AlMangour et al. [5] found that the scanning strategy has a significant influence on the parts densification, obtaining in their study the highest value in the 316L (reinforced with TiC nanoparticles) parts manufactured with a cross-hatched scanning strategy. On the other hand, they concluded that relatively strong crystallographic textures along the scanning and building directions can be transformed into weak, and the mechanical properties of the printed parts can be made nearly isotropic by rotating the scanning vector 90° between or inside the built layers. In addition, Larimian et al. [6] obtained the highest densification, the most refined microstructure and the best mechanical properties (Yield Tensile Strength (YTS), Ultimate Tensile Strength (UTS), elongation, and microhardness) for the 316L samples manufactured with the alternate hatches and single pass of laser beam. Salman et al. [7] showed that 316L parts manufactured with the "skin-core" scanning strategy achieved a finer microstructure, as well as the better combination of mechanical properties (YTS, UTS) than parts lacking this contour in the laser path. Rashid et al. [8] found that 17-4PH samples printed with double scanning strategy showed an improvement in relative density and hardness compared to those printed with single scanning. Regarding the geometrical accuracy of the manufactured parts, Zhang et al. [9] concluded that the "skin-core" scanning strategy results in Ti6Al4V circular parts with better precision than strategies that do not have this contour.

The influence of the rotation angle between successive layers for the normal scanning strategy has been much studied, particularly on texture, microstructure and properties of parts. Geiger et al. [10] demonstrated that the laser scanning angle can influence the crystallographic texture of IN738LC parts and, therefore, the anisotropy of its elastic properties. The results of the study by Liu et al. [11] showed that the scanning strategy used in the manufacture of reduced activation ferritic/martensitic steel parts influences the grain size and morphology of bimodal microstructure and, therefore, its mechanical properties. Dai et al. [12] evaluated the influence of scanning strategy with 90° rotation on the formation of the molten pool boundaries, microstructure, dimensional accuracy, tensile properties, microscopic sliding behaviour and fracture mechanism of AlSi12 parts. Wan et al. [13] also focused on analysing the influence of 90° rotation between successive layers, resulting in better mechanical properties (tensile and fatigue strength) for Inconel 718 parts when comparing to parts manufactured without scanning rotation between layers. Sun et al. [14] analysed the microstructure of the Ni25 at.%Mo alloy parts obtaining a single-

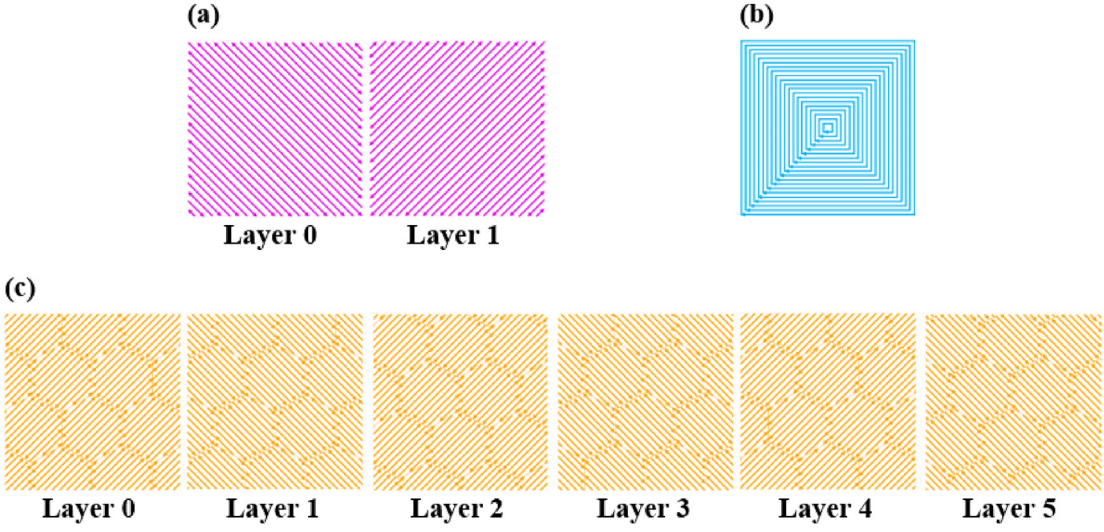

Fig. 1 – Laser scanning strategies used in SLM manufacturing of the test parts: (a) normal, (b) concentric and (c) hexagonal.

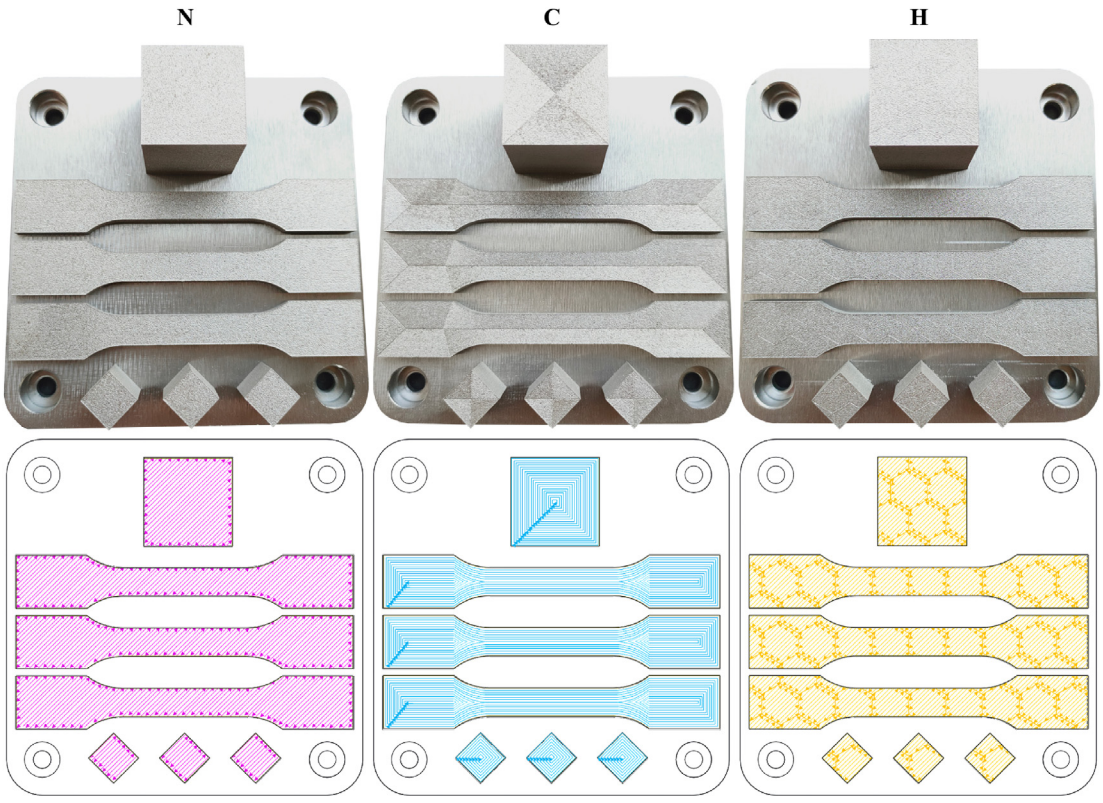

Fig. 2 – Manufactured test samples and graphical diagram of the laser path in the first layer for each scanning strategy (N, C and H).

crystalline-like texture for the parts manufactured without and with a 90° rotation between layers, while in the case of the parts manufactured with a 67° rotation a fibre texture was obtained. Similar results to the above were obtained by Marattukalam et al. [15] for 316L parts, resulting in a strong [100] and [110] single crystalline-like texture in the layer and build direction, respectively, for samples printed with a bidirectional scanning strategy without rotation. According to the study by Song et al. [16] the scanning strategy with 15° rotation generates higher stresses in Ti6Al4V parts than the strategy without rotation and with 90° rotation. Regarding the study of the characterization and mechanism of crack formation, Zhang et al. [17] concluded that strategies can effectively regulate grain morphology, texture and residual stress distribution to control cracks density and morphology. In the case of parts manufactured by SLM in FeCoCrNiMn high entropy alloy, lower crack densities were obtained with the normal strategy using a rotation angle of 67° [18].

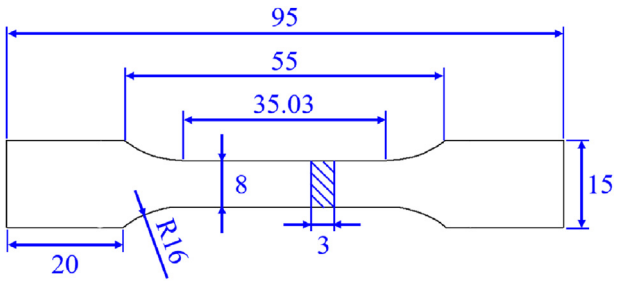

Fig. 3 – Dimensions of the tensile samples.

On the other hand, some researchers studied the effect of the normal strategy on SLM parts properties using simulations. Cao [19] concluded that pre-sintering results in parts with better properties in terms of grain orientation, pore defect and surface roughness. Parry et al. [20] recommend a scanning strategy design that avoids large scanning vector lengths and orients the direction of the vectors uniformly to produce an isotropic stress field in the part. They also indicate that the size of the hatch regions should be varied appropriately to maintain the highest temperature without causing instability in the process. In this way, the optimization of the scanning strategy could further mitigate the effects of residual stress and reduce the support structure requirements without requiring changes to the SLM machine or the manufactured part design [20]. Related to this, another research proposed a new scanning strategy (unidirectional scanning strategy in odd then even vectors sequence) aimed at reducing the level of residual stresses generated during the manufacturing process [21]. Jhabvala et al. [22] proposed a numerical model capable of detecting overheated zones or high temperature gradients to economically and efficiently assess the drawbacks and benefits of a given scanning strategy. On the other hand, Liang et al. [23] incorporate the effects of manufacturing with different scanning strategies into the modified inherent strain modelling framework to allow an accurate simulation for residual deformation of SLM metal parts.

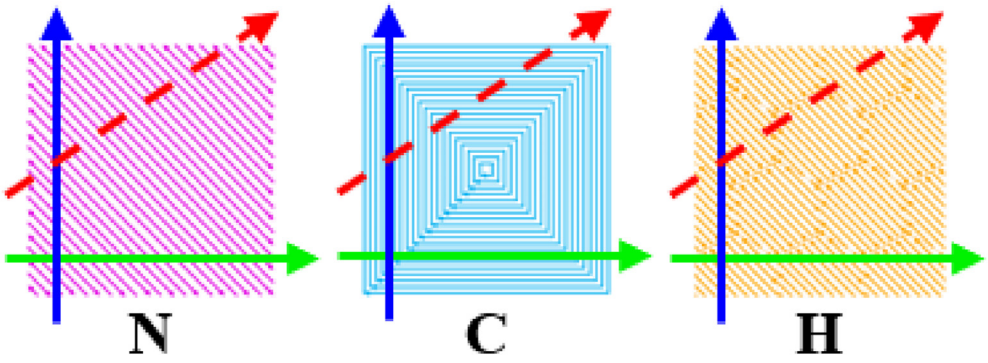

Fig. 4 – Roughness measurement directions on the top surface of the N, C and H samples.

In addition to the normal scanning strategy, the SLM manufactured parts have been evaluated using other laser strategies such as concentric [24] and island [25]. The island strategy with short vectors and a scanning direction rotated after each layer, breaks the large columnar grains into shorter and finer grain structures [3], leading to an improvement in tensile strength and good ductility of samples built using SLM technology [26]. Rotating the scanning vector between layers decreases the formation of residual stresses of SLM parts manufactured using the island strategy [27]. According to the results obtained by Zhang et al. [28], WC/Inconel 718 parts manufactured with the island strategy have low porosity, high microhardness and low wear rate. Wang et al. [29] also concluded that GH4169 samples manufactured using the chessboard scanning strategy have higher tensile strengths and more evident tensile anisotropy than samples manufactured using the normal strategy. Some researchers have studied the influence of island size on surface quality, microstructural characteristics, residual stress, tensile property or corrosion resistance in order to optimize the SLM process depending on the desired application for AlMgScZr [30] and Inconel 718 [31] parts. In addition to advantages of the island strategy, Zou et al. [32] concluded that the simultaneous application of four scanning lasers significantly reduces the residual stresses produced during the SLM process for the manufacture of Ti6Al4V parts. Another aspect that allows higher stress relief (regardless of the used scanning strategy) is the increase in the overlap area, due to the increase in re-melting [33]. On the other hand, Catchpole-Smith et al. [34], after analysing the island strategy, developed and experimentally tested new fractal scanning strategies based on the Hilbert and Peano-Gosper curves to SLM manufacturing of CM247LC superalloy parts.

The results obtained by other researchers show that the laser scanning strategy influences the quality of parts manufactured by SLM. So, to study the strategy influence is of great value for the manufacturing process in order to promote SLM technology in applications with high requirements. The properties of parts manufactured using different scanning strategies are also affected by the used material and the configuration of the rest of SLM parameters. In particular, there are not complete studies about the influence of the different scanning strategies on the quality of 17-4PH stainless steel parts used in SLM manufacturing, that is of great interest in sectors such as aerospace or automotive for its excellent mechanical properties. So far, research have only concluded that 17-4PH parts manufactured with the hexagonal strategy have higher hardness and better resistance to wear and

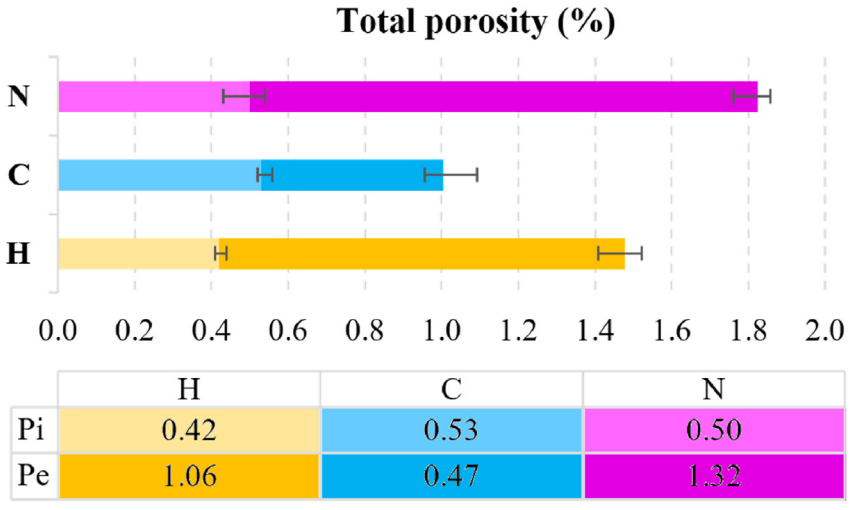

	H	C	N
Pi	0.42	0.53	0.50
Pe	1.06	0.47	1.32

Fig. 5 – Porosity values for the N, C and H strategies (P_i: internal porosity; P_e: external porosity).

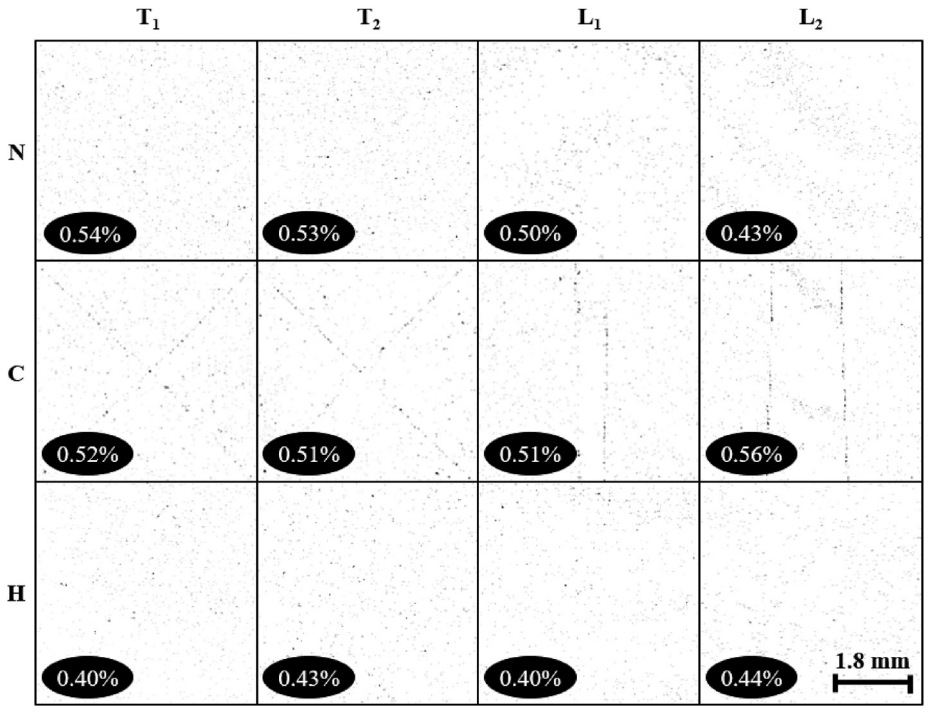

Fig. 6 – Analysis of internal porosity using ImageJ software on the T_1, T_2, L_1 and L_2 sections of the N, C and H samples.

corrosion than those manufactured with the concentric strategy [35]. Therefore, our research proposes to evaluate the 17-4PH manufactured parts using the three usual laser scanning strategies (normal, concentric and island) to optimize the SLM process depending on the final part application. As mentioned in the literature review of this section, the scanning strategy has a direct effect on the porosity, microstructure and mechanical properties of SLM parts, so it is proposed to include a porosity and microstructure analysis, as well as its effect on mechanical properties (hardness and tensile strength). Similarly, both the external porosity and the laser path in the last layers directly influence the surface quality of the printed parts. So, our research proposes also to analyse the roughness. In addition, the evaluation of the geometrical and dimensional quality of the parts is included in this research.

2. Materials and methods

2.1. *SLM manufacturing process and post-processes*

A 3DSystems ProX 100 SLM machine was used to manufacture the test parts from 17-4PH stainless steel powder (supplied by 3DSystems). Nitrogen was the gas used to inert the build chamber during the SLM process. The machine parameters of laser power (38 W) and focal distance (defocussing) were optimized in a previous work [36]. According to the manufacturer's recommendations, the rest of the main SLM parameters were setup to: 140 mm/s of scanning speed, a layer thickness of 30 μm and 70 μm of hatch distance. Regarding the scanning strategy parameter, the main interest in this study, the three strategies available in the manufacturing software were used. Fig. 1 shows the path followed by the laser beam during SLM manufacturing for the three used laser scanning strategies:

- **Normal (N)**: the laser beam traces a linear pattern with an inclination that changes from 45° to −45° in each layer as shown in Fig. 1a.
- **Concentric (C)**: the laser beam describes a trajectory bordering the geometry of the part from the outside to the inside of it (Fig. 1b).
- **Hexagonal (H)**: it is a type of island strategy, whose name is given by the hexagonal shape of the scanning patterns. As Fig. 1c shows, the hexagonal strategy is similar to the normal strategy (the linear direction of the laser beam trajectory changes from 45° to −45° in each layer) but in this case the laser beam melts the metallic powder hexagon to hexagon until the layer is completed. The hexagons position is repeated every three layers, the hexagon side size is 5000 μm and the overlap between them is 50 μm (standard values).

After the SLM manufacturing, the application of heat treatment for stress relieving is recommended, as it is the most effective method to relieve residual stresses [37]. Parts removed from the build-plate contain much lower stress levels than those that remain attached to it, but they suffer deformations during the split operation. Thus, stress relieving HT becomes highly relevant after SLM parts manufacturing and before cutting off them from the build-plate [38]. In addition, this HT post-processing is beneficial for homogenizing microstructure and improving the mechanical properties of SLM parts [39]. Therefore, the test parts were exposed

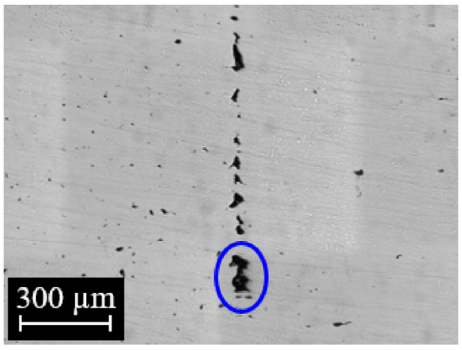

Fig. 7 – The largest pore (located in L_2 section of the C sample).

to HT for stress relieving. In this study, the stress relieving HT used for the 17-4PH stainless steel parts was 650 °C for 2 h and air cooling (following the manufacturer's recommendations). Finally, the parts were split from the build-plate by wire electrical discharge machining.

2.2. *Samples design and properties tests*

Various samples were designed to characterize the properties of the parts manufactured by SLM with the three scanning strategies mentioned in the previous section: N, C and H (Fig. 2). All of the tests described below were carried out on samples manufactured with these three SLM strategies. The dimensions of the build-plate are 100 mm × 100 mm. Fig. 2 shows the scanning pattern of the first layer for each manufactured set of parts. In the case of the C strategy, this pattern remains constant for all layers (making the anisotropic behaviour typical of AM even more noticeable). However, in parts manufactured using the N and H strategies, this pattern varies as shown in Fig. 1. In the N strategy, the scanning pattern is repeated every 2 layers (Fig. 1a), while in the H strategy it is repeated every 6 layers (Fig. 1c).

A 25 mm side cube was designed and manufactured to analyse the density/porosity using the Archimedes method. The mass of the sample was measured in air and in fluid with a CB-Complet precision electronic balance (precision of 0.001 g). The fluid used was demineralized water according to the recommendations of the study of Terris et al. [40] for SLM parts.

Two 10 mm side cubes were manufactured and then cut off using a metallographic cutting machine to analyse the porosity, microstructure and hardness inside the samples. One of them was cut off along the direction parallel to the manufactured layers, resulting in two samples of transversal section (T_1 and T_2). The other cube was cut off along the direction perpendicular to the manufactured layers, resulting in two samples of longitudinal section (L_1 and L_2). After cutting, the samples were encapsulated in resin and polished. For the analysis of internal porosity, mosaics of images that make up the polished internal surfaces of the cut samples (T_1, T_2, L_1 and L_2) were created and analysed using ImageJ software. These images were taken with an Olympus BHM-312 L Optical Microscope (OM) at ×50 magnifications. For the analysis of microstructure, the polished surface of T_1, T_2, L_1 and L_2 samples was etched with Vilella and images were taken with the OM at different magnifications. On the other hand, a Shimadzu HMW-2000 tester was used for the hardness tests according to ISO 6507-1 (2018) standard. Hardness tests were carried out at 9 points on the surface (distributed in a matrix of 2.5 mm equidistant points) following the Vickers HV2 procedure.

To evaluate the tensile strength, three tensile samples were designed according to the recommendations of ISO 6892-1 (2019) standard (Fig. 3). This test was carried out with the parameters' configuration for rectangular cross-section samples according to ISO 6892-1 (2019) using a Servosis ME-402/5 universal testing machine. In addition, images of fracture surfaces were taken after tensile test with a JEOL 6100 Scanning Electron Microscope (SEM).

In addition to the analysis of porosity (both internal and external), hardness and tensile strength, also the geometrical,

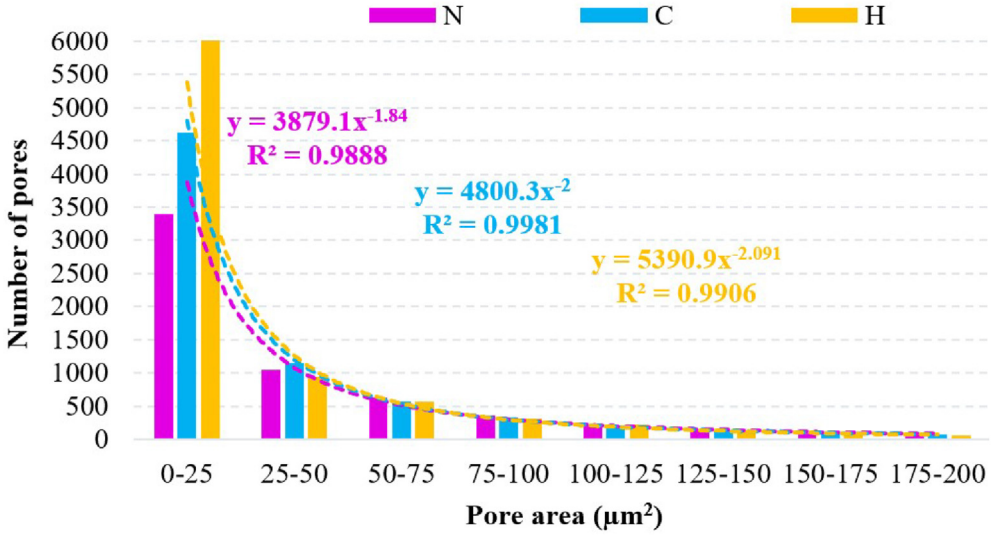

Fig. 8 – Number of pores as a function of pore size for N, C and H samples.

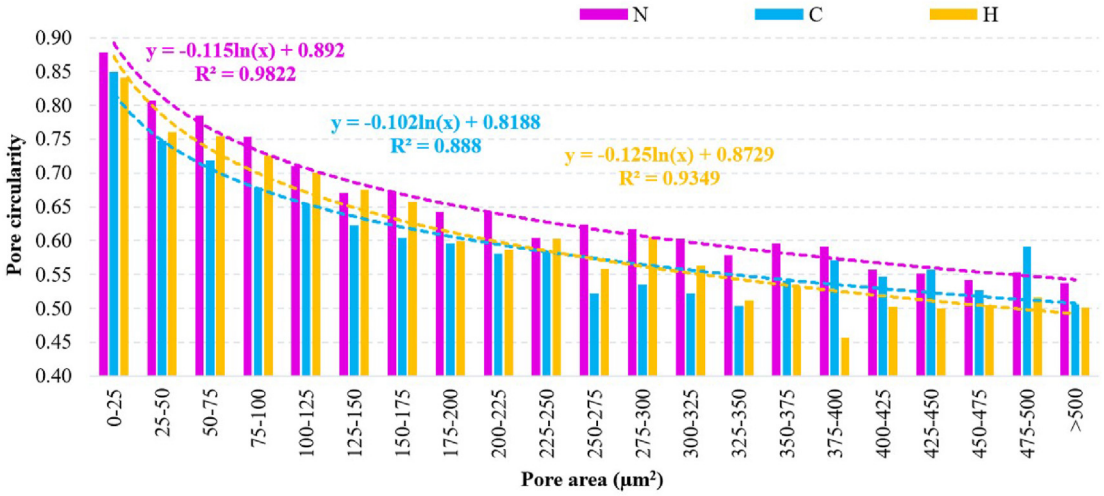

Fig. 9 – Pore circularity as a function of pore size for N, C and H samples.

dimensional and surface quality of the samples manufactured with the three scanning strategies was evaluated in order to determine the most appropriate SLM strategy according to the final application of the part.

The 25 mm cube was used to measure the roughness both at the top surface (corresponding to the surface finish resulting from SLM manufacturing with different scanning strategies) and at the lateral surfaces (corresponding to the surface finish resulting from the AM building process layer by layer). This test was performed with an SJ-500 Mitutoyo surface roughness measuring system equipped with a probe tip of 5 μm radius. The profile parameters of arithmetical mean roughness (R_a) and total height of the roughness profile (R_t) were measured for analysing the roughness. Measurements were taken on each of the cube faces using a sampling length of 2.5 mm and an evaluation length of 12.5 mm according to ISO 4288 (1996) standard. Due to the heterogeneity of the surface finish for the parts manufactured by SLM, 5 measurements were made on the top surface according to the horizontal (green arrow in Fig. 4), vertical (blue arrow in Fig. 4) and random (red arrow in Fig. 4) directions. On the lateral surfaces, 5 measurements were made according to the manufacturing direction and another 5 according to the layer direction.

A structured light scanner, model Breuckmann smartSCAN^{3D}-HE (currently AICON SmartScan), was used for the geometrical and dimensional analysis of the sample/build-plate set, since this system allows the precision optical inspection of this type of parts [41]. After calibrating the 3D scanner using the 125 mm field of view, the complete

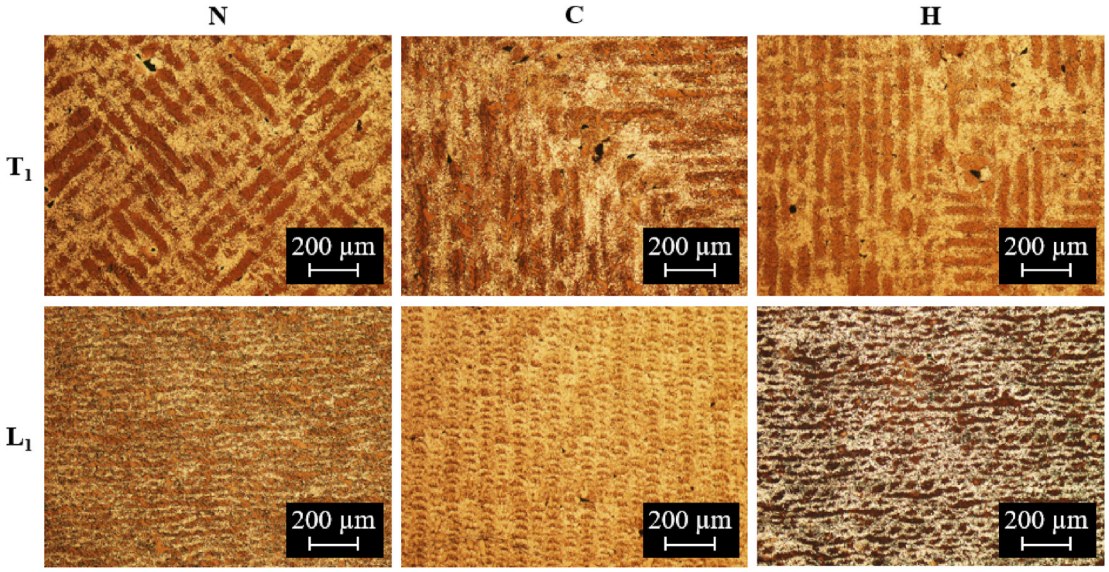

Fig. 10 – OM images with 100× magnification of the microstructure of T_1 and L_1 sections of the N, C and H samples.

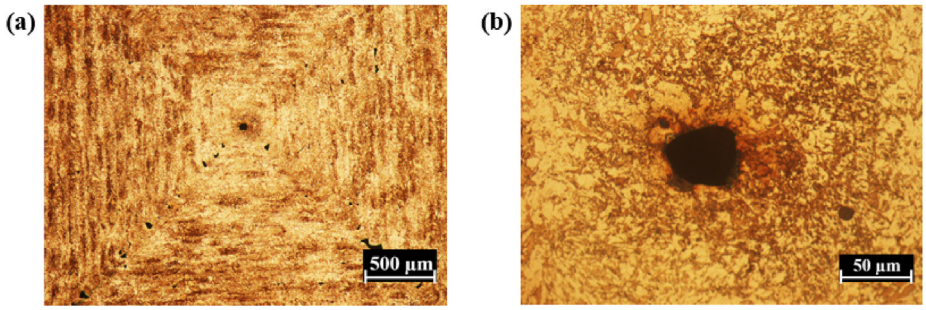

Fig. 11 – OM images of the microstructure of T_1 section of the C sample, taken with: (a) ×50 and (b) ×500 magnifications.

digitization of the samples was carried out. Data obtained from the 3D digitization (using the 3D scanner and the Optocat software) were processed in the advanced inspection software Geomagic Control X. The scanned data were imported into this software in *.stl format and the Best Fit alignment was used to aligned them with respect to the nominal CAD.

3. Results

3.1. *Density/porosity*

Fig. 5 shows the results of both closed/internal (P_i) and open/external (P_e) porosity of the analysed samples. The C sample presents the lowest level of P_e, about 0.5%, whereas for the other two strategies the value is higher than twice. The values of both types of porosity are very similar in the C sample. In the case of the N and H strategies, both show a P_e value significantly higher than P_i. Compared to the N strategy, the H strategy shows lower percentages for both types of porosity. Regarding the total porosity of the samples, the optimal result is obtained with the C strategy (1%), increasing this value to 1.48% and 1.82% for the H and N strategies, respectively. Consequently, the C samples have the highest density with 99%, compared to 98.52% (H) and 98.18% (N).

A binarization filter was applied in the ImageJ software to reveal the internal defects in the samples. Fig. 6 shows the results in the inner part surface for the transverse (T_1 and T_2) and longitudinal (L_1 and L_2) sections. The P_i values were similar for both the transversal and longitudinal sections of the samples. The percentage of internal porosity is not influenced either by the manufacturing direction (observed in the longitudinal sections) or by the layer direction (observed in the transversal sections).

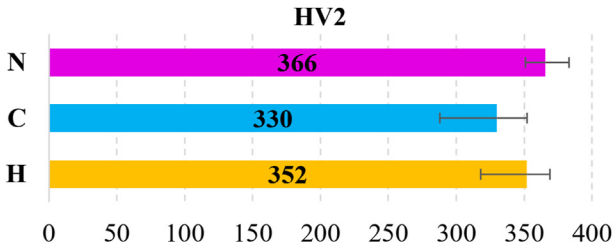

Fig. 12 – Hardness results on N, C and H samples.

It should be noted that the samples manufactured with the C strategy contains the largest pores. The formation of these large and irregularly shaped pores (Fig. 6) can be associated with the change of direction made by the laser during manufacturing with the C strategy (visible marks on the top surface of the samples as shown in Fig. 2). According to Tang et al. [24] this type of pores is the result of an inadequate melting of the metal powder and could be due to a decrease in the laser scanning speed at the time when its direction varies. This would lead to an instantaneous increase in the laser energy density and the generation of instability in the molten pools.

The samples analysis using the OM and the ImageJ software (Fig. 6) allowed to characterize the internal pores based on morphological aspects, such as their size and shape. In relation to pore size, the values vary highly from 0.50 μm^2 to 3331, 4460 and 9800 μm^2 for the H, N and C strategies, respectively. The largest pore, located in the longitudinal section of the C sample, has a completely irregular shape as shown in Fig. 7.

In all the analysed samples, the number of pores decreases as their size increases, perfectly fitting a potential function (Fig. 8). For the H strategy a 66% of the pores have a size smaller than 25 μm^2, in the case of the C strategy it is 61% and for the N strategy this percentage decreases to 53%. In accordance with these results, the H strategy has the lowest average pore size with a value of 42 μm^2, while the N and C strategies have the same value of 64 μm^2.

Pore circularity was other of the studied morphological aspect (Circularity $= 4\pi \cdot$Area/Perimeter^2). Although the H strategy was expected to have the greatest circularity (because it has an average pore size much smaller than the others), the three strategies have similar values of 0.82 (N), 0.79 (C) and 0.80 (H).

Circularity reaches higher values when the pore size decreases. The distribution of the pores circularity according to their size can be fitted to a logarithmic function (it decreases rapidly and then levels), as shown in Fig. 9 for the three scanning strategies. Regardless of the used strategy, pores with a size smaller than 25 μm^2 have the maximum circularity, with average values of 0.88 (N), 0.85 (C) and 0.84 (H). These smaller pores have a spherical or hemispherical shape and are usually the result of gases trapped in the molten pool

Table 1 – Hardness values for the T_1, T_2, L_1 and L_2 surfaces of N, C and H samples.

Section	N				C				H			
	Transversal		Longitudinal		Transversal		Longitudinal		Transversal		Longitudinal	
	T_1	T_2	L_1	L_2	T_1	T_2	L_1	L_2	T_1	T_2	L_1	L_2
HV2	366	359	367	372	320	322	339	339	354	357	346	352
Average	362		369		321		339		355		349	

due to excessive energy input and high cooling rates during the solidification process. As Fig. 9 shows, the pore irregularity increases as the pore size increases. In the case of pores that exceed 500 μm^2, the circularity reduces to average values of 0.54 (N), 0.51 (C) and 0.50 (H).

Analysing in more detail the perfect circular pores, that is, those whose circularity value is 1, it was determined that 22% of the pores for the N strategy are perfectly spherical, 23% for the case of the C strategy and 27% for the H strategy. The average size of these spherical pores was 6 (N), 5 (C) and 3 (H) μm^2, respectively.

3.2. *Microstructure*

Fig. 10 shows the microstructure of transversal (T_1) and longitudinal (L_1) sections of the samples manufactured with different scanning strategies after Vilella chemical etching. Transversal sections are characterized by laser trajectory marks, visible as parallel lines with a 90° change of direction (from 45° to −45°) between layers in the N and H strategies. While in the case of the C strategy, lines undergo changes of direction of 90° in the layer itself. Longitudinal sections reveal the molten pools resulting from the SLM manufacturing process. As concluded in previous studies [42], the molten pools interior is composed of martensite (dark colour) and the edge by austenite (light colour) (Fig. 10).

It is worth mentioning again the large pores contained in the samples manufactured with the C strategy. These pores are located mainly at the points where the laser beam abruptly changes direction according to an angle of 90° (Fig. 11a). As shown in Fig. 11b, this defect of lack of powder melting due the change of direction of the laser beam becomes greater in the sample centre, where a pore with an equivalent diameter of approximately 50 μm is produced.

3.3. *Hardness*

The hardness varies slightly for the three strategies, reaching average values of 366, 352 and 330 HV2 for the N, H and C samples, respectively (Fig. 12). As shown in Table 1, the mean value of nine measurements made on each sample is lower for C samples. This may be related to porosity, since the C strategy is the one that contains the largest pores. On the other hand, there is no notable trend between the hardness and the analysed section on the part. Hardness values obtained in the transversal directions (T_1 and T_2) are slightly lower than those obtained in the longitudinal ones (L_1 and L_2) in the N and C samples, while in the H samples the trend is inverse (Table 1).

3.4. *Tensile strength*

As shown Fig. 13, the results of tensile tests are very similar for the samples manufactured with the N and H strategy. The UTS value is practically the same, 1103 (N) and 1104 (H) MPa, while the YTS value is very close, 723 and 702 MPa in the N and H sample, respectively. Likewise, the stress–strain graphic follows the same trend in both strategies and the percentage of area reduction (Z) presents similar values, 29% (N) and 30% (H).

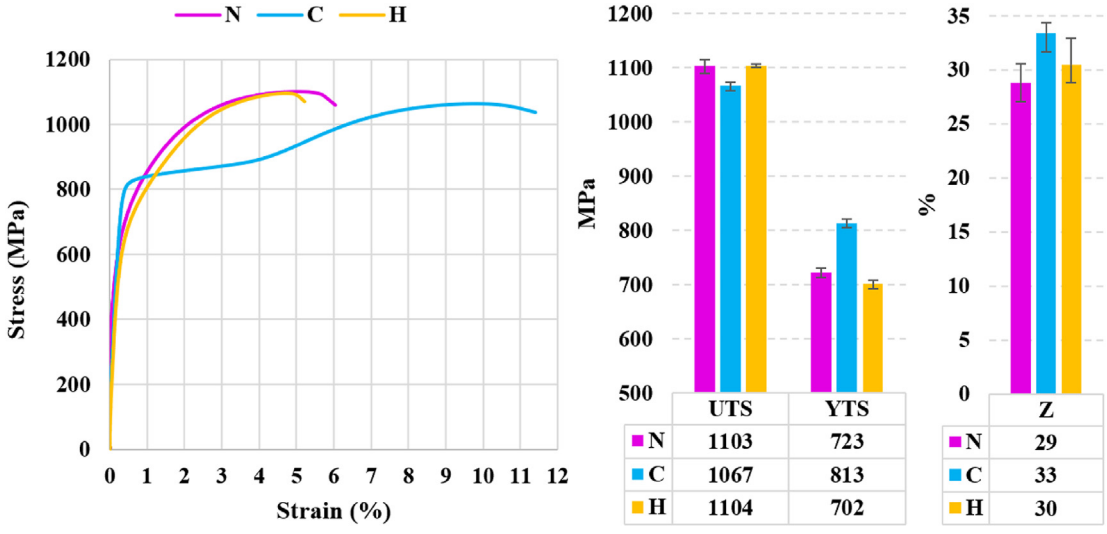

Fig. 13 – Tensile test results for the N, C and H samples (Stress–Strain graphic, UTS, YTS and Z).

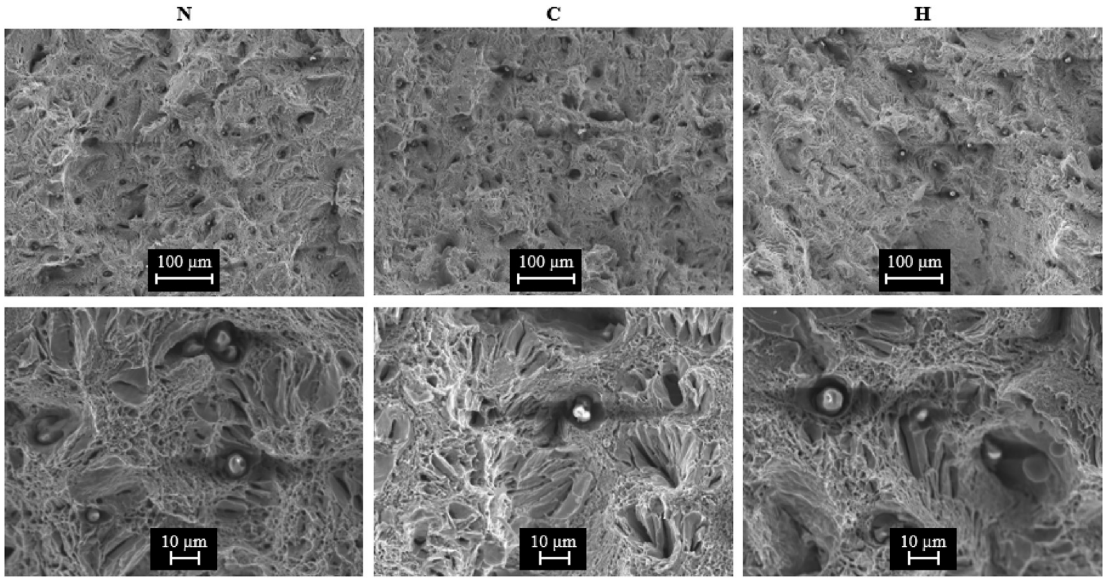

Fig. 14 – SEM images at 200× and 1000× magnifications of tensile fracture surfaces of the N, C and H samples.

On the other hand, the samples manufactured using the C strategy have slightly different values of UTS (1067 MPa), YTS (813 MPa) and Z (33%), and they show a very different stress–strain curve than the N and H samples (Fig. 13). These results are probably due to the scanning vectors direction. As shown in Fig. 2, the scanning vectors of the C tensile samples are large and describe the geometry completely outline. In addition, in the test area of the samples, these vectors have the same direction as the force applied in tensile test. Therefore, the tensile behaviour is observed so different in this strategy with respect to the others (N and H). Consequently, it would be interesting to study this property in samples with other geometries (such as cylindrical) manufactured using the C strategy.

The SEM images of tensile fracture surfaces of the samples N, C and H (Fig. 14) show pores, inclusions and spatter particles, which directly cause the nucleation of voids until their union and, finally, the rupture. The analysis of several images showed no significant differences in the distribution, size or shape of the voids between the samples manufactured with the different laser scanning strategies.

3.5. *Surface roughness*

The results of the roughness analysis show influence of both the scanning strategy used for SLM manufacturing (N, C, H) and the measured surface (top or lateral). Regarding the top surface, the lowest roughness values are obtained for the N samples and the highest for the C samples (Fig. 15a). In the case of lateral surfaces (Fig. 15b), the roughness is slightly reduced for the N and H strategies. On the other hand, a notable decrease is observed in the samples printed with the C

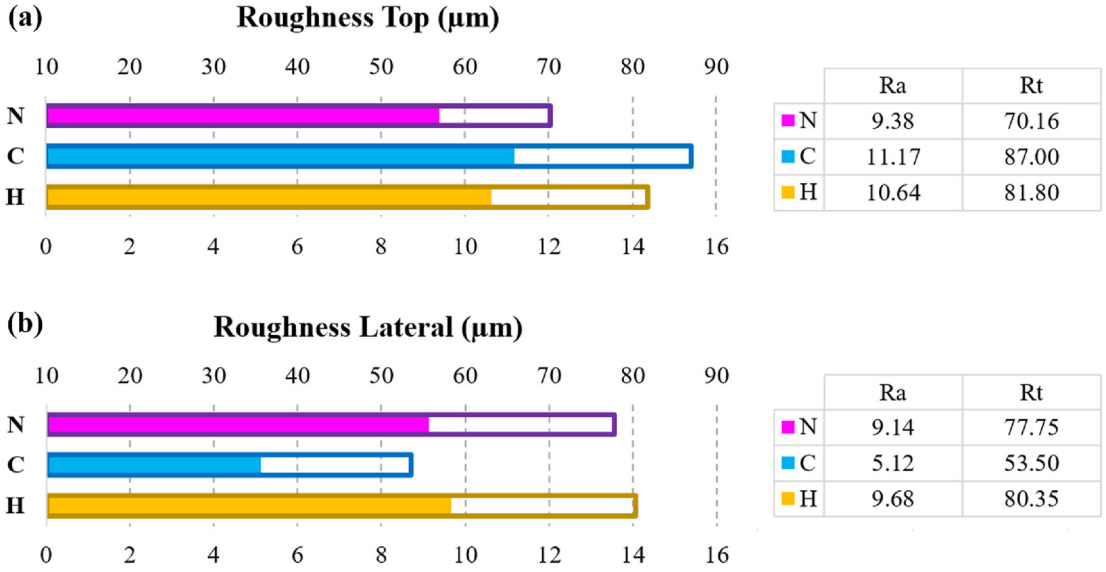

	Ra	Rt
N	9.38	70.16
C	11.17	87.00
H	10.64	81.80

	Ra	Rt
N	9.14	77.75
C	5.12	53.50
H	9.68	80.35

Fig. 15 – Roughness results (R_a and R_t) for (a) top and (b) lateral faces of N, C and H samples.

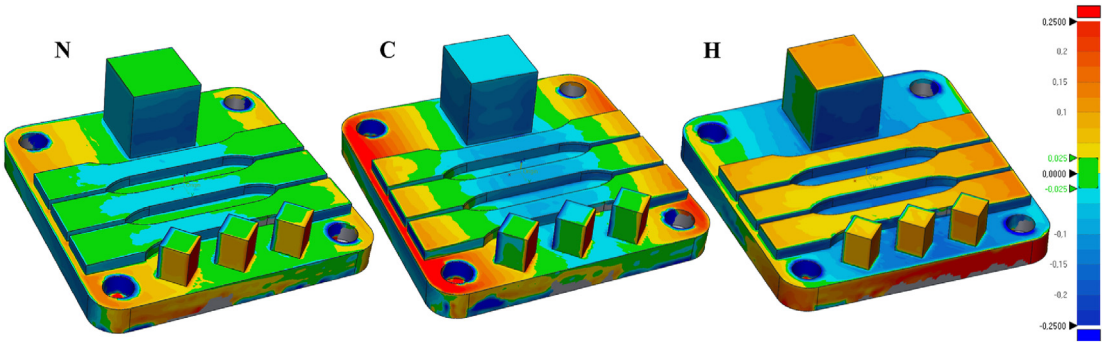

Fig. 16 – 3D comparison between the designed nominal CAD and the sample/build-plate set scanned point clouds.

strategy, reaching the lowest value for both R_a (5.12 μm) and R_t (53.50 μm) parameters (Fig. 15b). From these results it can be concluded that the concentric laser trajectory, identical in each manufacturing layer (Fig. 1b), produces the best surface finish on lateral surfaces. These results are consistent with the low external porosity obtained in the C samples (Fig. 5).

3.6. *Geometrical and dimensional accuracy*

This section shows the results of the geometrical and dimensional analysis for the N, C and H samples. Fig. 16 shows the 3D comparison between the designed nominal CAD and the point clouds that result from scanning the samples (N, C and H) on the build-plate. The green colour indicates the best-fitting surfaces between the nominal CAD and the SLM manufactured parts. The 3D comparison results reveal a slight concave shaped deformation of the build-plate after the SLM process. This effect is more pronounced in the C strategy and, in particular, in the larger and thinner samples (tensile samples), mainly due to their large scanning vectors (Fig. 2). This may be due to the thermal gradient suffered by parts printed with this strategy, which results in residual compression stresses in the central area of the parts and tensile stresses at the edge, difficult to eliminate completely with heat treatment.

Fig. 17 shows the results of the geometrical (flatness and perpendicularity) and dimensional (XY size) analysis of the samples manufactured using the different laser scanning strategies (N, C, H). The perpendicularity of the cubic samples was calculated as the error between their lateral faces and their upper XY face (taken as reference).

Regardless of the laser scanning strategy used in SLM manufacturing, the flatness and perpendicularity errors of the cubic samples are similar (Fig. 17a). However, it is worth noting the significant increase in geometrical error in the manufacture of large samples (tensile samples), as well as the

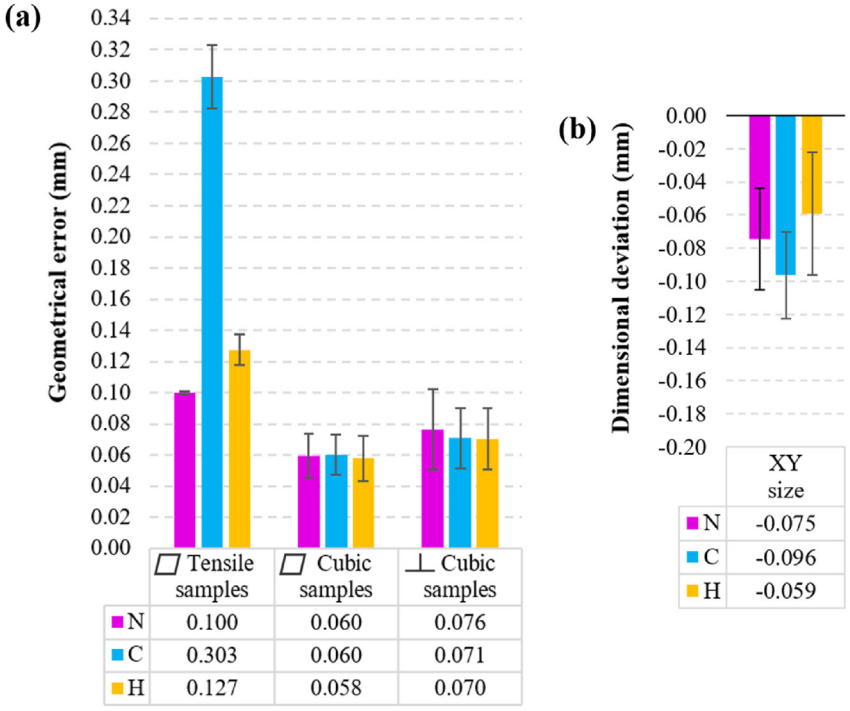

Fig. 17 – Results of (a) geometrical and (b) dimensional analysis of N, C and H samples.

influence of the used strategy. For the N and H strategies, tensile samples resulted in flatness errors of less than 105 μm (N) and 140 μm (H). While the large samples printed with the C strategy presented high flatness errors (303 μm ± 20 μm), mainly due to the large length of the scanning vectors travelled by the laser during SLM manufacturing.

Regarding the dimensional analysis of the cubic samples (Fig. 17b), the three strategies present a decrease in the XY size. The resulting mean values are approximately −60 μm (H), −75 μm (N) and −95 μm (C).

4. Conclusions

In order to analyse the influence of the laser scanning strategy used in SLM manufacturing on the quality of 17-4PH stainless steel parts, this paper focuses on the evaluation of SLM manufactured parts using the normal (N), concentric (C) and hexagonal (H) strategies. Manufacturing material (density and microstructure), mechanical (hardness and tensile strength), geometrical and dimensional, as well as surface (roughness) properties were evaluated. The following conclusions have been drawn to select the most appropriate SLM manufacturing scanning strategy based on the part application and according to the analysed properties.

The H sample can be considered the most appropriate in terms of porosity due to the characteristics of its pores (size and shape) as well as for presenting the lowest percentage of internal porosity. On the other hand, the C samples have the lowest total porosity, despite containing the largest pores. These large and irregular pores are located in the area where the laser changes direction during the scanning, according to the C strategy for each powder layer. Therefore, it is of interest to analyse the porosity of cylindrical samples manufactured by SLM using the C strategy, thus avoiding the sudden change of direction of the laser trajectory.

Regarding the mechanical properties, the strategy slightly influences both the tensile behaviour and the hardness. The N and H samples present a similar tensile behaviour, reaching values close to 1100 MPa of UTS, 712 MPa of YTS and 30% of area reduction. Likewise, the stress–strain curve is very similar in these two strategies, but completely different to the obtained with the C strategy. In the C strategy, a more ductile behaviour is shown, and accordingly, it has lower hardness than the N and H strategies.

Regarding the surface finish, notable differences were observed between the top (corresponding to the surface finish resulting from scanning strategy) and lateral (corresponding to the surface finish resulting from the AM manufacturing process layer by layer) surfaces of the C samples. These samples present the highest roughness values on the top face and the smallest values on the lateral faces. The N and H strategies have similar values on both the top and lateral surfaces, reaching slightly lower values in the case of the N samples.

In general, the N and H strategies provide lower geometrical and dimensional errors. On the other hand, SLM manufacturing using the C strategy produces high geometrical errors, especially in parts with large scanning vectors. Consequently, it is recommended to avoid the C strategy to manufacture large and thin components with high geometrical and dimensional requirements.

The surface roughness values obtained on the SLM printed parts using the three strategies (N, C and H) are not an exact match of their surface topology. Several industrial applications demand parts with high surface finish requirements, so post-process operations are necessary. Some of them, such as sand-blasting post-process, reduces the surface roughness and the external porosity. Therefore, we consider of interest to study the influence of SLM strategies on the quality of parts subjected to different post-processes, in order to optimize the entire manufacturing process.

On the other hand, we are analysing the manufacture of SLM parts combining these scanning strategies in order to obtain the best mechanical properties for the core of the parts and the most adequate surface finish for the shell.

Declaration of Competing Interest

The authors declare that they have no known competing financial interests or personal relationships that could have appeared to influence the work reported in this paper.

Acknowledgments

The authors gratefully acknowledge the financial support provided by the Junta de Castilla y León and FEDER (project ref. LE027P17).

REFERENCES

[1] DebRoy T, Wei HL, Zuback JS, Mukherjee T, Elmer JW, Milewski JO, et al. Additive manufacturing of metallic components – process, structure and properties. Prog Mater Sci 2018;92:112–224. https://doi.org/10.1016/j.pmatsci.2017.10.001.

[2] Cheng B, Shrestha S, Chou K. Stress and deformation evaluations of scanning strategy effect in selective laser melting. Addit Manuf 2016;12:240–51. https://doi.org/10.1016/j.addma.2016.05.007.

[3] Nong XD, Zhou XL. Effect of scanning strategy on the microstructure, texture, and mechanical properties of 15-5PH stainless steel processed by selective laser melting. Mater Char 2021;174:111012. https://doi.org/10.1016/j.matchar.2021.111012.

[4] Gu D, Chen H. Selective laser melting of high strength and toughness stainless steel parts: the roles of laser hatch style and part placement strategy. Mater Sci Eng A 2018;725:419–27. https://doi.org/10.1016/j.msea.2018.04.046.

[5] AlMangour B, Grzesiak D, Yang JM. Scanning strategies for texture and anisotropy tailoring during selective laser melting of TiC/316L stainless steel nanocomposites. J Alloys Compd 2017;728:424–35. https://doi.org/10.1016/j.jallcom.2017.08.022.

[6] Larimian T, Kannan M, Grzesiak D, AlMangour B, Borkar T. Effect of energy density and scanning strategy on densification, microstructure and mechanical properties of 316L stainless steel processed via selective laser melting.

Mater Sci Eng A 2020;770:138455. https://doi.org/10.1016/j.msea.2019.138455.
[7] Salman OO, Brenne F, Niendorf T, Eckert J, Prashanth KG, He T, et al. Impact of the scanning strategy on the mechanical behavior of 316L steel synthesized by selective laser melting. J Manuf Process 2019;45:255–61. https://doi.org/10.1016/j.jmapro.2019.07.010.
[8] Rashid R, Masood SH, Ruan D, Palanisamy S, Rahman Rashid RA, Brandt M. Effect of scan strategy on density and metallurgical properties of 17-4PH parts printed by Selective Laser Melting (SLM). J Mater Process Technol 2017;249:502–11. https://doi.org/10.1016/j.jmatprotec.2017.06.023.
[9] Zhang L, Zhang S, Zhu H. Effect of scanning strategy on geometric accuracy of the circle structure fabricated by selective laser melting. J Manuf Process 2021;64:907–15. https://doi.org/10.1016/j.jmapro.2021.02.015.
[10] Geiger F, Kunze K, Etter T. Tailoring the texture of IN738LC processed by selective laser melting (SLM) by specific scanning strategies. Mater Sci Eng A 2016;661:240–6. https://doi.org/10.1016/j.msea.2016.03.036.
[11] Liu CY, Tong JD, Jiang MG, Chen ZW, Xu G, Liao HB, et al. Effect of scanning strategy on microstructure and mechanical properties of selective laser melted reduced activation ferritic/martensitic steel. Mater Sci Eng A 2019;766:138364. https://doi.org/10.1016/j.msea.2019.138364.
[12] Dai D, Gu D, Zhang H, Xiong J, Ma C, Hong C, et al. Influence of scan strategy and molten pool configuration on microstructures and tensile properties of selective laser melting additive manufactured aluminum based parts. Opt Laser Technol 2018;99:91–100. https://doi.org/10.1016/j.optlastec.2017.08.015.
[13] Wan HY, Zhou ZJ, Li CP, Chen GF, Zhang GP. Effect of scanning strategy on mechanical properties of selective laser melted Inconel 718. Mater Sci Eng A 2019;753:42–8. https://doi.org/10.1016/j.msea.2019.03.007.
[14] Sun SH, Hagihara K, Nakano T. Effect of scanning strategy on texture formation in Ni-25 at.%Mo alloys fabricated by selective laser melting. Mater Des 2018;140:307–16. https://doi.org/10.1016/j.matdes.2017.11.060.
[15] Marattukalam JJ, Karlsson D, Pacheco V, Beran P, Wiklund U, Jansson U, et al. The effect of laser scanning strategies on texture, mechanical properties, and site-specific grain orientation in selective laser melted 316L SS. Mater Des 2020;193:108852. https://doi.org/10.1016/j.matdes.2020.108852.
[16] Song J, Wu W, Zhang L, He B, Lu L, Ni X, et al. Role of scanning strategy on residual stress distribution in Ti-6Al-4V alloy prepared by selective laser melting. Optik 2018;170:342–52. https://doi.org/10.1016/j.ijleo.2018.05.128.
[17] Zhang C, Feng K, Kokawa H, Han B, Li Z. Cracking mechanism and mechanical properties of selective laser melted CoCrFeMnNi high entropy alloy using different scanning strategies. Mater Sci Eng A 2020;789:139672. https://doi.org/10.1016/j.msea.2020.139672.
[18] Guo L, Gu J, Gan B, Ni S, Bi Z, Wang Z, et al. Effects of elemental segregation and scanning strategy on the mechanical properties and hot cracking of a selective laser melted FeCoCrNiMn-(N,Si) high entropy alloy. J Alloys Compd 2021;865:158892. https://doi.org/10.1016/j.jallcom.2021.158892.
[19] Cao L. Mesoscopic-scale numerical investigation including the influence of scanning strategy on selective laser melting process. Comput Mater Sci 2021;189:110263. https://doi.org/10.1016/j.commatsci.2020.110263.
[20] Parry L, Ashcroft IA, Wildman RD. Understanding the effect of laser scan strategy on residual stress in selective laser melting through thermo-mechanical simulation. Addit Manuf 2016;12:1–15. https://doi.org/10.1016/j.addma.2016.05.014.
[21] Ramos D, Belblidia F, Sienz J. New scanning strategy to reduce warpage in additive manufacturing. Addit Manuf 2019;28:554–64. https://doi.org/10.1016/j.addma.2019.05.016.
[22] Jhabvala J, Boillat E, Antignac T, Glardon R. On the effect of scanning strategies in the selective laser melting process. Virtual Phys Prototyp 2010;5:99–109. https://doi.org/10.1080/17452751003688368.
[23] Liang X, Dong W, Chen Q, To AC. On incorporating scanning strategy effects into the modified inherent strain modeling framework for laser powder bed fusion. Addit Manuf 2021;37:101648. https://doi.org/10.1016/j.addma.2020.101648.
[24] Tang X, Zhang S, Zhang C, Chen J, Zhang J, Liu Y. Optimization of laser energy density and scanning strategy on the forming quality of 24CrNiMo low alloy steel manufactured by SLM. Mater Charact 2020;170:110718. https://doi.org/10.1016/j.matchar.2020.110718.
[25] Javidrad HR, Ghanbari M, Javidrad F. Effect of scanning pattern and volumetric energy density on the properties of selective laser melting Ti-6Al-4V specimens. J Mater Res Technol 2021;12:989–98. https://doi.org/10.1016/j.jmrt.2021.03.044.
[26] Song Y, Sun Q, Guo K, Wang X, Liu J, Sun J. Effect of scanning strategies on the microstructure and mechanical behavior of 316L stainless steel fabricated by selective laser melting. Mater Sci Eng A 2020;793:139879. https://doi.org/10.1016/j.msea.2020.139879.
[27] Ali H, Ghadbeigi H, Mumtaz K. Effect of scanning strategies on residual stress and mechanical properties of Selective Laser Melted Ti6Al4V. Mater Sci Eng A 2018;712:175–87. https://doi.org/10.1016/j.msea.2017.11.103.
[28] Zhang H, Gu D, Ma C, Guo M, Wang R, Yang J, et al. Microstructure and tribological property of selective laser melted Ni-based composites using different scanning strategies. Vacuum 2020;177:109439. https://doi.org/10.1016/j.vacuum.2020.109439.
[29] Wang YC, Lei LM, Shi L, Wan HY, Liang F, Zhang GP. Scanning strategy dependent tensile properties of selective laser melted GH4169. Mater Sci Eng A 2020;788:139616. https://doi.org/10.1016/j.msea.2020.139616.
[30] Zhang H, Gu D, Dai D, Ma C, Li Y, Peng R, et al. Influence of scanning strategy and parameter on microstructural feature, residual stress and performance of Sc and Zr modified Al–Mg alloy produced by selective laser melting. Mater Sci Eng A 2020;788:139593. https://doi.org/10.1016/j.msea.2020.139593.
[31] Lu Y, Wu S, Gan Y, Huang T, Yang C, Junjie L, et al. Study on the microstructure, mechanical property and residual stress of SLM Inconel-718 alloy manufactured by differing island scanning strategy. Opt Laser Technol 2015;75:197–206. https://doi.org/10.1016/j.optlastec.2015.07.009.
[32] Zou S, Xiao H, Ye F, Li Z, Tang W, Zhu F, et al. Numerical analysis of the effect of the scan strategy on the residual stress in the multi-laser selective laser melting. Results Phys 2020;16:103005. https://doi.org/10.1016/j.rinp.2020.103005.
[33] Sing SL, Yeong WY. Laser powder bed fusion for metal additive manufacturing: perspectives on recent developments. Virtual Phys Prototyp 2020;15:359–70. https://doi.org/10.1080/17452759.2020.1779999.
[34] Catchpole-Smith S, Aboulkhair N, Parry L, Tuck C, Ashcroft IA, Clare A. Fractal scan strategies for selective laser melting of 'unweldable' nickel superalloys. Addit Manuf 2017;15:113–22. https://doi.org/10.1016/j.addma.2017.02.002.
[35] Lashgari HR, Xue Y, Onggowarsito C, Kong C, Li S. Microstructure, tribological properties and corrosion behaviour of additively manufactured 17-4PH stainless steel: effects of scanning pattern, build orientation, and single vs.

Double scan. Mater Today Commun 2020;25:101535. https://doi.org/10.1016/j.mtcomm.2020.101535.
[36] Zapico P, Giganto S, Martínez-Pellitero S, Fernández-Abia AI, Castro-Sastre MÁ. Influence of laser energy in the surface quality of parts manufactured by selective laser melting. Ann DAAAM Proc Int DAAAM Symp 2018;0279–86. https://doi.org/10.2507/29th.daaam.proceedings.040.
[37] Li C, Liu ZY, Fang XY, Guo YB. Residual stress in metal additive manufacturing. Procedia CIRP 2018;71:348–53. https://doi.org/10.1016/j.procir.2018.05.039.
[38] Mercelis P, Kruth JP. Residual stresses in selective laser sintering and selective laser melting. Rapid Prototyp J 2006;12:254–65. https://doi.org/10.1108/13552540610707013.
[39] Anant Pidge P, Kumar H. Additive manufacturing: a review on 3 D printing of metals and study of residual stress, buckling load capacity of strut members. Mater Today Proc 2020;21:1689–94. https://doi.org/10.1016/j.matpr.2019.12.012.
[40] de Terris T, Andreau O, Peyre P, Adamski F, Koutiri I, Gorny C, et al. Optimization and comparison of porosity rate measurement methods of Selective Laser Melted metallic parts. Addit Manuf 2019;28:802–13. https://doi.org/10.1016/j.addma.2019.05.035.
[41] Giganto S, Martínez-Pellitero S, Cuesta E, Meana VM, Barreiro J. Analysis of modern optical inspection systems for parts manufactured by selective laser melting. Sensors 2020;20. https://doi.org/10.3390/s20113202.
[42] Leo P, Cabibbo M, Prete A Del, Giganto S, Martínez-Pellitero S, Barreiro J. Laser defocusing effect on the microstructure and defects of 17-4ph parts additively manufactured by slm at a low energy input. Metals 2021;11:588. https://doi.org/10.3390/met11040588.